RSC Advances

PAPER

View Article Online
View Journal | View Issue

Cite this: *RSC Adv.*, 2017, **7**, 52738

Preparation of Cu(II) porphyrin–TiO_2 composite in one-pot method and research on photocatalytic property†

Xin Zhao,‡ Ying Wang,‡ Wenhua Feng, Hengtao Lei and Jun Li*

Received 29th August 2017
Accepted 1st November 2017

DOI: 10.1039/c7ra09585f

rsc.li/rsc-advances

A promising fabrication strategy used for designing TiO_2 photocatalysts, which enhanced the photocatalytic activity by combining TiO_2 with a new carboxyl-group-containing Cu(II) porphyrin (CuPp) in a sol–gel processing TiO_2 and a one-pot solvothermal condition, has been proposed. Both porphyrins and composite photocatalyst CuPp–TiO_2 have been characterized by spectroscopic techniques. Their photocatalytic performances were investigated by testing the photodegradation of 4-nitrophenol (4-NP) in aqueous solution under UV-vis light irradiation. The results reveal that the methodology for the anatase TiO_2 photocatalyst is easy to achieve, and the photocatalytic activity measurements illustrate that the Cu(II) porphyrin-based TiO_2 photocatalyst we synthesized displays superior photocatalytic activity and good chemical stability for organic pollutant photodegradation due to the strong interactions between Cu(II) porphyrins and TiO_2.

1. Introduction

TiO_2-based photocatalytic processes can be used in various applications such as waste water treatment, gas purification and environmental protection[1–3] due to its nontoxicity, good chemical stability, high photocatalytic activity and versatile properties.[4–7] In addition, it has shown a great potential as an inexpensive, environmentally friendly and sustainable treatment technology to remove pollutants from sewage to overcome the shortcomings of the conventional technologies.[8,9] However, the utilization for solar energy is limited by the narrow band gap of light absorption region in TiO_2,[10,11] which impedes its commercialization. To improve the photocatalytic efficiency of TiO_2, many techniques[12,13] have been carried out with the aim of eliminating the inefficient exploitation of visible light for TiO_2. The synthesis of excellent photocatalytic TiO_2 materials with heterogeneous structure, which is extensively considered to possess higher photocatalytic activity,[14] may have profound implications for organic dye pollutant photodegradation.

Porphyrins, as the most promising components, have been widely used in the field of gas sorption, molecular separation, storage, and catalysis.[15–17] Their photophysical properties can be easily tuned by metal ion insertion, since porphyrins are able to coordinate with metal ions readily in the central cavity causing stronger and broader photoresponse in the visible region. It is for this reason, that porphyrins are considered to be efficient sensitizers to harvest light on the surface of TiO_2.[18,19] In particular, ideally designed Cu(II) porphyrins–TiO_2 composites were found to be more effective sensitizers in the photodegradation of organics,[20,21] which could not only extend the absorption range in the solar spectrum, but also enhance the separation of photogenerated electron–hole pairs, thus increasing activity and stability in the photocatalytic processes of the porphyrin–TiO_2 system.

Studies have shown that metal complexes of porphyrins are highly photostable when adsorbed on the surface of TiO_2.[18,22] The sol–gel process allows the direct introduction of visible light sensitive species like porphyrins inside the TiO_2 matrix with ease during the synthesis.[23,24] The heterogenous structure formation is advantageous to environmental applications. Herein, we report a route for the synthesis of a novel Cu(II) carboxyl porphyrin (Fig. 1) *via* a sol–gel process and in solvothermal conditions (Fig. 2), which helps in the easy realization of the efficient porphyrin–TiO_2 photocatalyst. The CuPp–TiO_2 composite has been characterized with spectroscopic techniques, N_2 sorption and 4-nitrophenol (4-NP) degradation, which reveals that the heterogeneous CuPp–TiO_2 composite exhibits potential visible photocatalytic activity and higher recyclability than P25, thus, making our synthetic route a prospective method for the preparation of highly efficient and stable porphyrin–TiO_2 photocatalysts.

Key Laboratory of Synthetic and Natural Functional Molecule Chemistry of Ministry of Education, College of Chemistry & Materials Science, Northwest University, Xi'an, Shaanxi 710069, P. R. China. E-mail: junli@nwu.edu.cn

† Electronic supplementary information (ESI) available: Integral TEM images of (a) TiO_2, (b) CuPp–TiO_2 photocatalyst (Fig. S1). Corresponding EDX element mapping of CuPp–TiO_2 composite photocatalyst (j) for carbon, (k) for oxygen, (l) for titanium, (d) for nitrogen, (e) for copper (Fig. S2). The degradation efficiency of 4-NP in the presence of CuPp–TiO_2 composite photocatalyst with scavengers (Fig. S3). See DOI: 10.1039/c7ra09585f

‡ These authors contributed equally to this work.

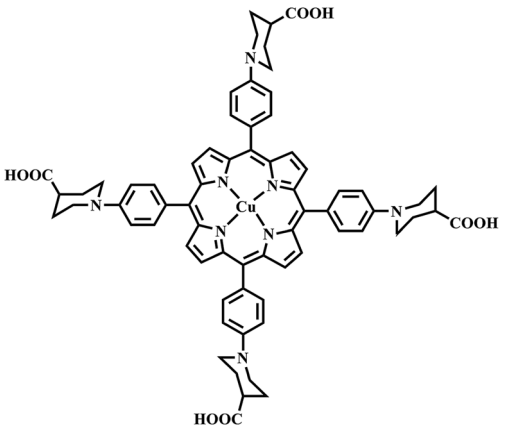

Fig. 1 Chemical structure of CuPp.

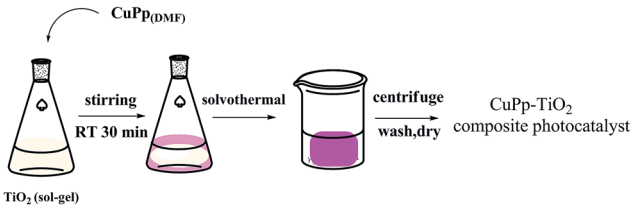

Fig. 2 The preparation of CuPp–TiO_2 composite photocatalyst with sol–gel procedure and solvothermal conditions.

2. Experimental

2.1 Materials, reagents and equipment

All reagents and solvents used were purchased from commercial sources and used without further purification except pyrrole, which was distilled before use.

UV-vis diffuse reflectance spectra (UV-vis-DRS) were recorded on a Shimadzu UV-3100 system using $BaSO_4$ as a reference. Mass spectrometry (MS) analyses were carried out on a matrix assisted laser desorption/ionization time of flight mass spectrometer (MALDI-TOF MS, Krato Analytical Company of Shimadzu Biotech, Manchester, Britain). Elemental analyses (C, H and N) were performed by Vario EL-III CHNOS instrument. The Powder X-ray diffraction (XRD) was examined with a Bruker D8 diffractometer using graphite monochromatic copper radiation (Cu-Kα) at 40 kV and 30 mA over the 2θ range 5–80°. FT-IR spectra were recorded on a BEQUNDX-550 spectrometer on samples embedded in KBr pellets. The surface property of the sample was determined by XPS *via* Axis Ultra, Kratos (UK) using monochromatic Al K radiation (150 W, 15 kV, 1486.6 eV). Model XPA-VII photocatalytic reactor with a halogen lamp as the light source (Xujiang Electromechanical Plant, Nanjing, China) was employed to evaluate the degradation of 4-NP.

2.2 Synthesis of porphyrins

2.2.1 Synthesis of ester porphyrins H_2Pp–OMe, CuPp–OMe. The synthetic routes of 5, 10, 15, 20-tetrakis(4-(4-carboxylic)piperidyl) phenyl porphyrin are shown in Fig. 3. The detailed procedures were as follows: 5, 10, 15, 20-tetrakis(4-(4-formatemethyl)piperidyl) phenyl porphyrin (H_2Pp–OMe) was prepared *via* the well-known Adler-Longo method:[25] 1-(4-aldehydephenyl) piperidine-4-carboxylic acid (3.7068 g, 15 mmol) was dissolved in propionic acid (90 mL) with vigorous stirring at 140 °C, and newly distilled pyrrole (1 mL, 15 mmol) in propionic acid (10 mL) was added dropwise in 30 min. The solvent was removed after another 1 h reaction. Furthermore, 20 mL ethanol was added and cooled to room temperature. Then, the mixture was filtrated under vacuum and purified by chromatography on a silica gel column using 2% ethanol of CH_2Cl_2 as the eluent to produce H_2Pp–OMe as a purple solid.

Yield: 11%. Mp: >250 °C. Anal. calcd (found) for $C_{72}H_{74}N_8O_8$ (mol. wt: 1179.41), %: C 73.63 (73.32); H 6.91 (6.32); N 8.97 (9.50); O 10.49 (10.86). MS: *m*/*z*: 1180.57 ($M + H^+$) amu. UV-vis (CH_2Cl_2), λ_{max}/nm, 431 (Soret band), 523, 568, 656 (Q bands). ^{1}HNMR (400 MHz, $CDCl_3$): δ (ppm) = 8.88 (m, 8H, β-H), 8.09 (d, 4H, Ar), 7.29 (d, 4H, Ar), 3.98–3.08 (t, 16H, α-H), 3.78 (s, 12H, –$COOCH_3$), 2.67–2.58 (m, 4H, –CHC═O–), 2.24–2.01 (m, 16H, β-H), −2.68 (s, 2H, N-H). FT-IR (KBr): υ, cm^{-1}, 3379, 2937, 2803, 1730, 1607, 1515, 1311, 1192, 1042, 922, 804.

An excess of ten times of $Cu(OAc)_2$ (0.2 g) and H_2Pp–OMe (0.1785 g) was dissolved separately in ethanol (20 mL) and CH_2Cl_2 (20 mL) with stirring at room temperature for 12 h. TLC was checked at the conclusion of the reaction. After removing the unreacted solid salt and solvent, the crude product was chromatographed on a silica column with dichloromethane as the eluent, a purple solid of CuPp–OMe was obtained.

Yield: 86%. Mp: >250 °C. $C_{72}H_{72}CuN_8O_8$ (mol. wt: 1240.94), %: C 70.27 (69.69); H 6.01 (5.85); N 9.02 (9.03); O 9.97 (10.31); Cu 4.73 (5.12). MS: *m*/*z* 1241.48 ($M + H^+$) amu. UV-vis (CH_2Cl_2) λ_{max}/nm, 430 (Soret band), 545 (Q band). FT-IR (KBr): υ, cm^{-1}, 2951, 1728, 1600, 1503, 1304, 1187, 1045, 920, 802.

2.2.2 Synthesis of CuPp. The synthesis of CuPp is similar to the method previously reported in the literature:[26] CuPp–OMe was mixed with 1 mol L^{-1} aqueous KOH (20 mL) using THF as the solvent heated to reflux at 66 °C for 48 h. Additional water was added to the resulting water phase until the solid was completely dissolved, and then the solution was acidified with HCl (1 mol L^{-1}) until no further precipitate appeared (pH = 3). The precipitated solid was filtered and washed with distilled water. Finally, the compound CuPp was obtained after vacuum drying at 80 °C for 6 h.

Yield: 86%. Mp: >250 °C. $C_{68}H_{64}CuN_8O_8$ (mol. wt: 1184.83), %: C 69.33 (68.93); H 5.36 (5.44); N 9.25 (9.46); O 10.27 (10.80); Cu 5.79 (5.37). MS: *m*/*z* 1185.41 ($M + H^+$) amu. UV-vis (DMF) λ_{max}/nm, 432 (Soret band), 547, 591 (Q bands). FT-IR (KBr): υ, cm^{-1}: 3413, 1704, 1602, 1505, 1102, 938, 802.

2.3 Preparation of TiO_2 nanometer photocatalyst

The preparation procedure of TiO_2 sol nanometer photocatalyst is given below: in the first step, anhydrous ethanol (30 mL) tetrabutyltitanate (10 mL, 29.4 mmol) and acetic acid (2 mL) were mixed together at room temperature under continuous stirring. Then, nitric acid (0.5 mL), H_2O (1 mL) and anhydrous

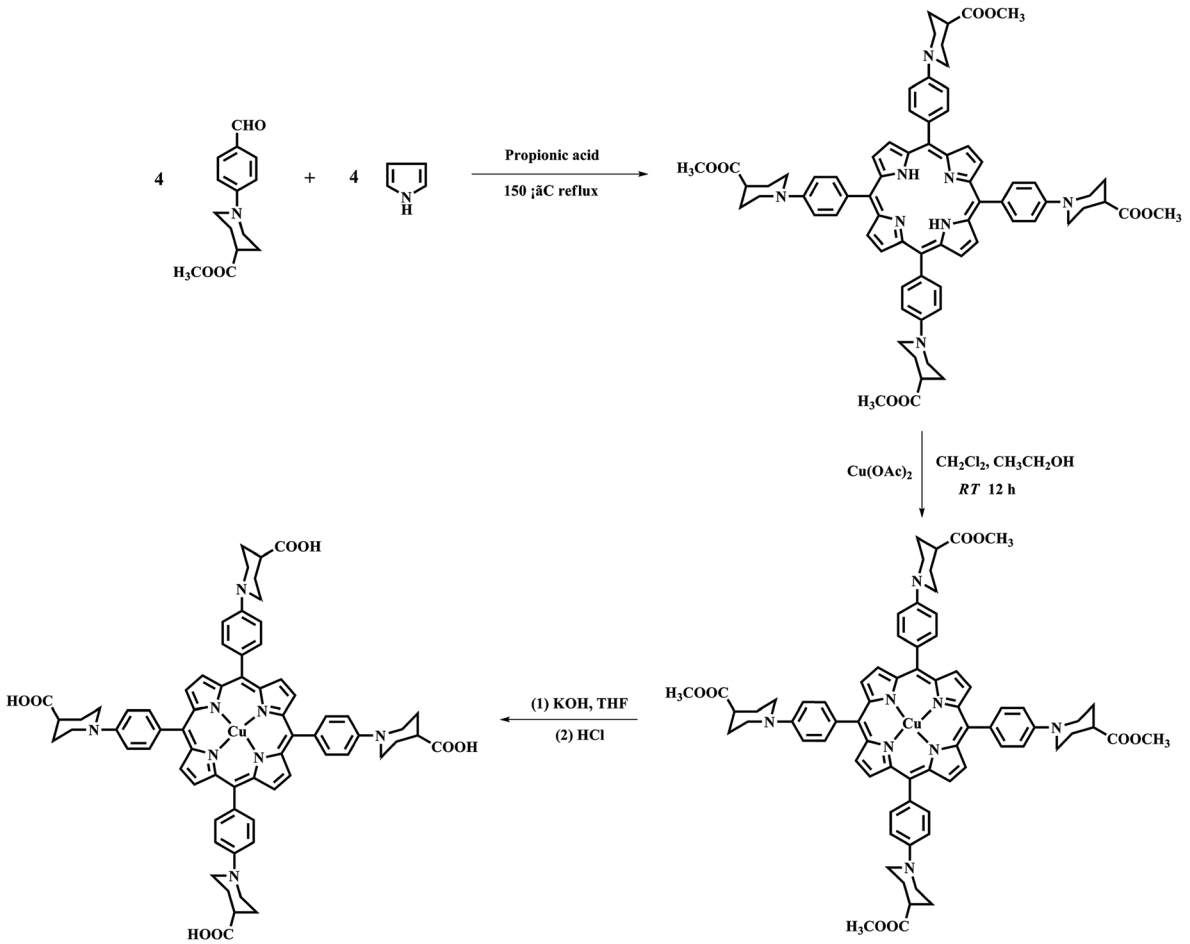

Fig. 3 Synthesis of the H_2Pp–OMe, CuPp–OMe and CuPp.

ethanol (10 mL) was added dropwise to the above solution for 1.5 h. After that, a translucent TiO_2 sol was obtained.

Second, 6 drops of water were added to 5 mL of TiO_2 sol, and the mixture was stirred for 30 min. Then, the mixture was transferred into a 25 mL Teflon-lined autoclave casing at 90 °C and heated to 150 °C for 24 h. A gel like photocatalyst was obtained after cooling to room temperature. The sample was washed with anhydrous ethanol several times and soaked for 24 h. Finally, TiO_2 nanoparticles were fabricated after being dried and ground.

2.4 The synthesis of CuPp–TiO_2 photocatalyst

The preparation procedure of mesoporous CuPp–TiO_2 was similar to that of TiO_2 nanometer photocatalyst synthesis, except that the CuPp load was increased: 0.0175 g amount of as-prepared CuPp was dissolved in 6 mL DMF. TiO_2 (5 mL) was added dropwise to the solution of CuPp–DMF (2 mL), and distilled water (0.3 mL) was added to the mixed solution severally. Then, the solvothermal condition was analogous to that mentioned above.

2.5 Photocatalytic activity tests

The photoreactivity experiments were carried out using a Model XPA-VII photocatalytic reaction instrument according to the previous report:[27] 10 mg photocatalysts were added into 50 mL 4-NP (1×10^{-4} mol L^{-1}) solution. The suspension was stirred vigorously with air bubbled when irradiating by 400 W of the central light source. The photocatalysis lasted for 60 min, and every 6 min we took out 3 mL sample of the suspension. The photocatalysts were separated from the solution by centrifugation, and the quantity of 4-NP was measured by its absorption at 317 nm with a Shimadzu UV-1800 UV-vis-NIR system.

2.6 Stability of the photocatalyst

The stability test for CuPp–TiO_2 photocatalyst was carried out following a procedure similar to that used for the photodegradation of 4-NP. The experimental procedure and test conditions were the same as those mentioned above; the experiments were repeated six times. Catalysts for each test were collected by centrifugation, washed with distilled water, and dried in a vacuum oven after every photocatalytic cycle experiment.

2.7 Photocatalytic mechanism investigation

Active species trapping experiment was employed to detect reactive species in photocatalysis process, which was carried out with the same procedure as that for the photodegradation test, except for the addition of selected scavengers. Benzoquinone (BQ, 0.2 mM), ammonium oxalate (AO, 10 mM), and isopropyl

alcohol (IPA, 10 mM) were selected as scavengers of superoxide anionic radicals ($^{\bullet}O_2^-$), photoinduced holes (h^+) and hydroxyl radicals ($^{\bullet}OH^-$), respectively.

3. Results and discussions

3.1 Morphology analysis

The surface morphology of the TiO_2 and CuPp–TiO_2 photocatalyst can be seen in Fig. 4a and c from the SEM images. It can be observed that the microsphere of CuPp–TiO_2 possesses a similar appearance as the TiO_2 we prepared previously. Integral TEM images shown in Fig. S1† show that the composite has a microsphere structure, which indicates that the CuPp molecules on the surface of TiO_2 particles have no effect on the size and shape of the TiO_2 powders.

The high resolution transmission electron microscopy (HRTEM) images of TiO_2, which was synthesized with a sol–gel procedure under solvothermal conditions, are shown in Fig. 4b to exhibit the crystal lattice indices of {001} and {101}, which is typical of anatase TiO_2.[28–31] Therefore, it can be concluded that the crystallization processes, as further confirmed by XRD measurements, occur uniformly *via* the strategy. CuPp–TiO_2 photocatalyst illustrated in Fig. 4d shows a heterojunction structure, which exists as two different types of lattice fringes in the CuPp–TiO_2 composite: the narrow fringe spacing (about 0.36 nm) could be assigned to the {101} planes of anatase TiO_2. Moreover, a wider lattice spacing of about 0.71 nm is also observed, which may come from the crystal plane of CuPp.[32,33] This verified that CuPp deposited well onto the surface of TiO_2 nanoparticles and permeated readily into the spaces among the nanoparticles.[34] This may be ascribed to the infiltration of CuPp in the process of high-temperature solvothermal synthesis. These observations show that the preservation of CuPp crystals significantly modified the crystal structure of the TiO_2. Furthermore, we created massively intrinsic channels for photoproduced holes and electrons. Thereby, CuPp–TiO_2 composite photocatalyst with a heterojunction structure is capable of displaying superior photocatalytic activity, which is in a good agreement with the photocatalytic experimental results.

3.2 XRD analysis

X-ray diffraction (XRD) measurements were conducted to investigate the crystal phase of CuPp–TiO_2 particles and the effect of CuPp on the crystal structure of TiO_2. As shown in Fig. 5, there is almost no difference between CuPp–TiO_2 and TiO_2. XRD spectra taken in 2θ configuration have exhibited peaks at 25.3°, 38.3°, 48.0°, 54.2°, 63.4°, 69.1° and 75.5°, and they can be indexed to the (1 0 1), (0 0 4), (2 0 0), (1 0 5), (2 1 1), (2 0 4), and (2 1 5) lattice planes reflection of anatase TiO_2 (JCPDS card 21-1272),[35] which gives higher photocatalytic activity than rutile and brookite.[36,37] The CuPp diffraction fringe fails to display owing to the infinitesimal amount of CuPp on the surface of TiO_2, indicating that the CuPp loaded on the surface of TiO_2 microsphere could scarcely transform the intrinsic crystal of TiO_2.

3.3 UV-vis-DRS analysis

The UV-visible diffuse-reflectance (UV-vis-DRS) spectra were measured in the range of 200–800 nm in order to explore the

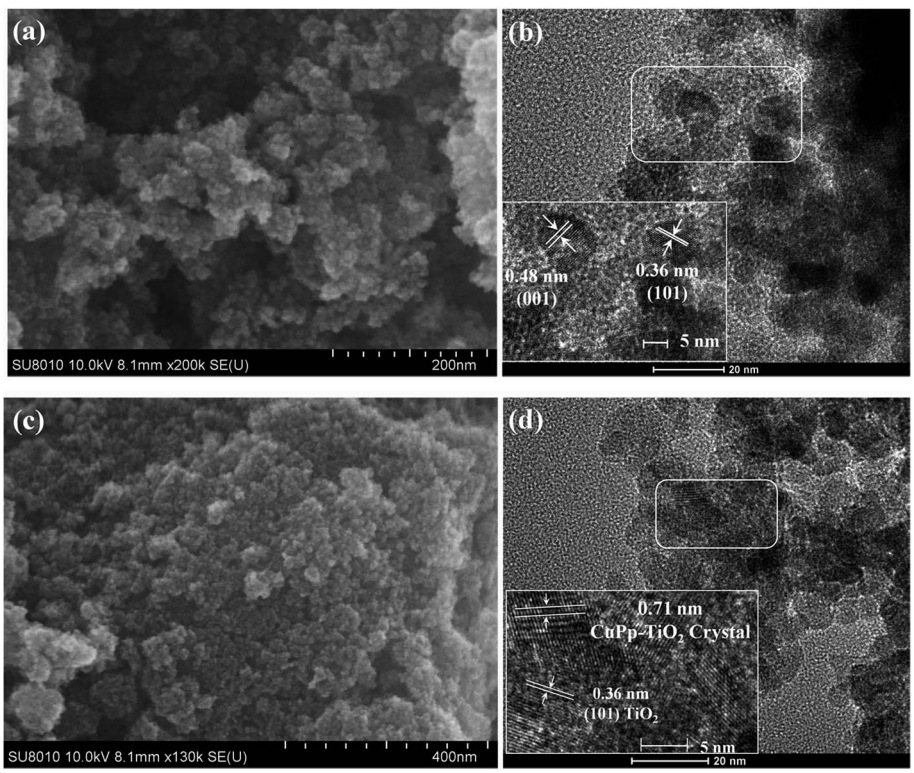

Fig. 4 SEM and TEM images of TiO_2 (a), (b); CuPp–TiO_2 composite (c), (d).

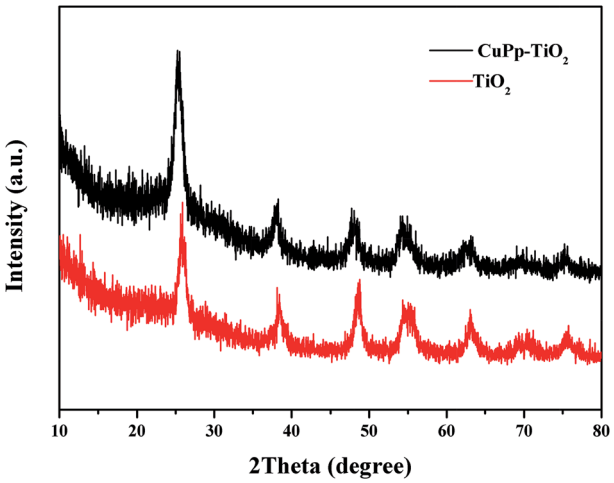

Fig. 5 XRD patterns of TiO_2, and CuPp–TiO_2 composite.

optical response of TiO_2 and CuPp–TiO_2. As shown in Fig. 6, no obvious absorption peaks were observed above 400 nm for TiO_2. However, CuPp–TiO_2 photocatalyst, which exhibited peaks typical of CuPp, demonstrated that the CuPp might influence the band width of TiO_2. This proves that the CuPp unit was perfectly impregnated onto the surface of TiO_2. As a result, the CuPp–TiO_2 photocatalyst expanded the absorption range for the solar spectrum in comparison with TiO_2. It is noticed that the Soret and Q bands of the CuPp–TiO_2 are slightly blue-shifted and broadened relative to CuPp in a DMF solution, implying that CuPp in CuPp–TiO_2 photocatalyst had adopted a type H stack mode.[38] The band gap energies can be determined by extrapolating the absorption edge onto the energy axis (shown in Fig. 6 insertion), wherein the conversion of the reflectance to absorbance data was obtained by the Kubelka–Munk function (K–M).[39,40] The band gap energies of TiO_2 and CuPp–TiO_2 samples are 3.23 and 3.18 eV, respectively.

3.4 FT-IR spectra analysis

The FT-IR spectra were used to verify the interaction between CuPp and TiO_2. As shown in Fig. 7, there exists a broad characteristic vibration band of Ti–O around 707 cm^{-1}. The disappearance of the C=O stretching vibration of the carboxyl group in CuPp molecules around 1705 cm^{-1} and the new band at around 1650 cm^{-1} and the weak absorptions at around 1406 cm^{-1} in CuPp–TiO_2 might be ascribed to the emergence of asymmetric and symmetric stretch of $-COO^-$. Therefore, this serves as sufficient evidence that CuPp is able to be chemisorbed on the surface of TiO_2. Moreover, enhancement of electron transferring between CuPp and Ti orbital manifold of TiO_2 can be tuned by O=C–O–Ti bonds.[41,42] The appearance of C–O–Ti and C=O groups in CuPp–TiO_2, which were provided with polarity, resulted in asymmetric electronic structures, contributing to the improvement of photocatalytic activity further.

3.5 XPS analysis

X-ray Photoelectron Spectroscopy (XPS) analyses were used to investigate the surface chemical states and composition change of TiO_2 and CuPp–TiO_2. Fig. 8 showed the XPS spectra of both TiO_2 and CuPp–TiO_2. The survey spectra (Fig. 8a) show that the CuPp–TiO_2 composite contains the Cu, Ti, O and C, while TiO_2 consists of Ti and O, which was consistent with the corresponding EDX-measured elemental maps (Fig. S2†). The element of C for TiO_2 mainly comes from adventitious carbon-based contaminants. There is an enhancement of the C 1s peak intensity in CuPp–TiO_2, which may attributed to the massive amounts of adsorbed CuPp molecules. As for Ti 2p spectra (Fig. 8b), the Ti $2p_{3/2}$ binding energy of the CuPp–TiO_2 (465.0 eV) is higher than that of the TiO_2 sample (464.7 eV); this suggested that the Ti atom of the TiO_2, as the acceptor, coordinates with the O atom of CuPp as the donor, *i.e.* Ti atom of the TiO_2 adopted the electrons of the O atom in the carbonyl group (O–C=O) from CuPp molecules,[43,44] which is in agreement with the FT-IR results. As a result, the electron cloud density of O atom in CuPp decreased and is accompanied with an increased valence for the O atom, and consequently an increased binding energy of O 1s (530.8 eV) (Fig. 8c) compared to that of TiO_2 (530.2 eV).[45] Moreover, the peaks located at 934.1 and 954.1 eV (ref. 46) also

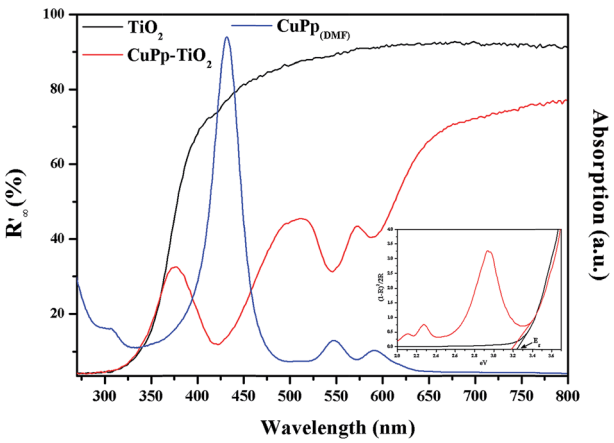

Fig. 6 UV-vis-DRS spectra of TiO_2 (black line), CuPp–TiO_2 (red line) composite and UV-vis spectrum of CuPp (blue line), the insertion is the Kubelka–Munk function.

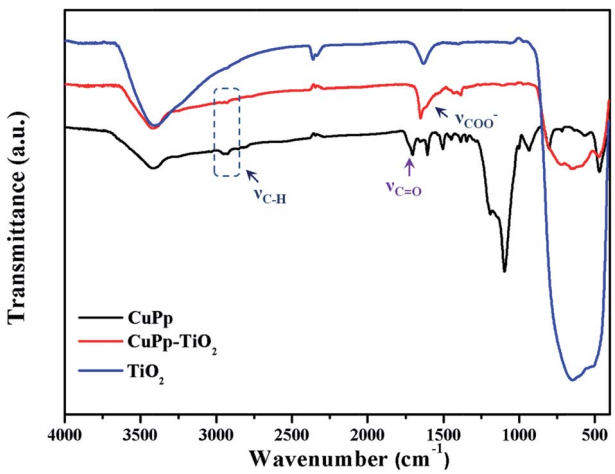

Fig. 7 The FT-IR spectra of CuPp, CuPp–TiO_2, TiO_2 composite.

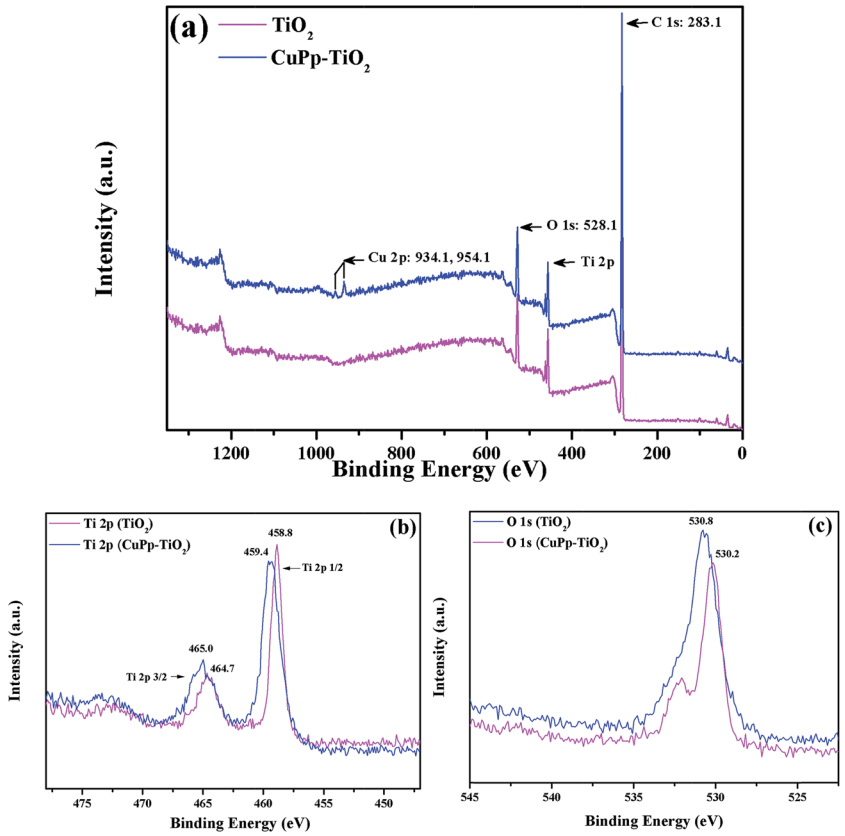

Fig. 8 XPS spectra of the TiO_2 and CuPp–TiO_2 composite photocatalyst, (a) survey spectra, (b) Ti 2p spectra, (c) O 1s spectra.

imply the presence of CuPp in CuPp–TiO_2 composite, indicating CuPp molecules adsorbed on the TiO_2 nanoparticle surface.

3.6 BET analysis

N_2 adsorption analyses were used to evaluate the porous properties of the samples. Fig. 9 demonstrated the nitrogen adsorption–desorption isotherm and pore size distribution curve of TiO_2 and CuPp–TiO_2 composite. The pore size distribution is calculated from the desorption branch of a nitrogen isotherm by the Barrett–Joyner–Halenda (BJH) method.[47] The samples exhibit a type IV adsorption isotherm with a hysteresis loop according to IUPAC classifications, whose adsorption branch of the isotherm is not consistent with the desorption branch, indicating that both of them are typical characteristics of a mesoporous structure.[48] The detailed tested data are summarized in Table 1. The as-prepared TiO_2 and CuPp–TiO_2 possessed high BET specific surface area of 127.89–140.57 $m^2\ g^{-1}$, which are far higher than those of commercial TiO_2 (anatase, BET specific surface area 8 $m^2\ g^{-1}$).

3.7 Photocatalytic activity analysis

The photocatalytic activities were assessed by the degradation of organic dyes 4-nitrophenol (4-NP) in aqueous solution under white light illumination. P25, the mixture of CuPp and TiO_2 serve as references for investigating photocatalytic activities. Fig. 10 shows the photocatalytic efficiency of all samples compared to the blank test, which contained 4-NP(aq) only. As expected, all samples exhibit relatively effective photocatalytic ability in comparison with the blank test. P25 exhibits a favorable performance in photocatalytic activity, whereas the CuPp–TiO_2 composite photocatalyst displays a higher removal rate in 4-NP photocatalytic degradation. As such, the CuPp–TiO_2 composite photocatalyst manifests inherent superior catalytic

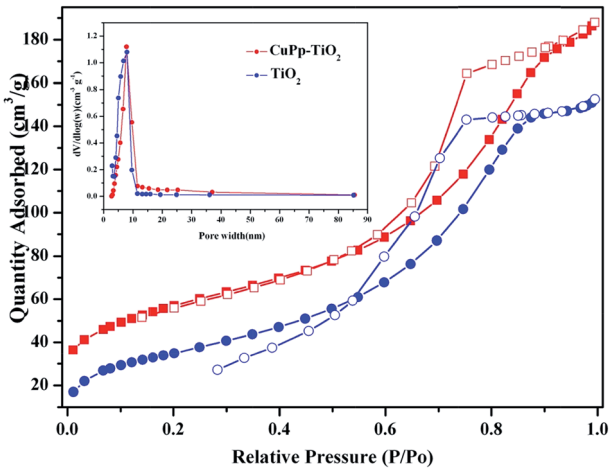

Fig. 9 N_2 adsorption (solid symbols)–desorption (open symbols) isotherms of TiO_2 and CuPp–TiO_2 composite. The inset picture was pore size distribution.

Table 1 The detailed pore information of mesoporous TiO_2 and CuPp–TiO_2

Samples	BET (m^2 g^{-1})	Pore width (nm)	V_{BJH} (cm^3 g^{-1})
TiO_2	127.89	7.21	0.32
CuPp–TiO_2	140.57	7.15	0.29

activity to the mixture of CuPp and TiO_2, which confirmed that it is the heterojunction structures formed by sol–gel progress and solvothermal conditions that improve the efficiency of the photoreactivity process.

3.8 The repeatability test

The photostability and reusability are important indicators to measure the practical performance of the catalyst. The study of CuPp–TiO_2 reproducibility in photocatalytic degradation of 4-NP was carried out to evaluate stability of CuPp–TiO_2 composite. As can be seen in Fig. 11, 100% 4-NP was removed in the first run, and the degradation efficiency decreased gradually with increasing cycle times. The catalytic efficiency of CuPp–TiO_2 composite for the next five cycles was reduced to 93.3%, 88.5%, 85.6%, 81.5% and 78.1% respectively, indicating the photocatalytic activity did not obviously decrease within six cycles of reutilization, which exhibited relatively high stability in photodegradation. The stability test confirmed that the CuPp dispersed on the surface of TiO_2 exhibited remarkable stability under irradiation, because of the interactions between Cu(II) porphyrin and TiO_2 in CuPp–TiO_2 composite photocatalyst.

3.9 Mechanism explanation

Active species trapping experiment has been carried out to detect the active species in accordance with previous reports.[49,50] It has been widely known that the hydroxyl radicals ($^{\bullet}OH$), superoxide anion radicals ($^{\bullet}O^{2-}$) and photogenerated holes (h^+) are the main active species in the photocatalysis process,[51,52] which can be detected through the trapping experiment with scavengers isopropyl alcohol (IPA), benzoquinone (BQ) and ammonium oxalate (AO) respectively.[53–55] As shown in Fig. 12, the degradation efficiency of 4-NP is changed slightly with the addition of AO as a h^+ scavenger, indicating that h^+ does not dominate the photodegradation progress. On the contrary, the degradation percentage reduced to a certain extent with the participation of IPA and TBA, which served as $^{\bullet}OH$ scavengers. The degradation activity is dramatically inhibited after the addition of BQ, which inferred that $^{\bullet}O^{2-}$ is the main active species in 4-NP photocatalytic degradation (Fig. S3†). It can therefore be concluded that 4-NP degradation was inhibited to some degree by the addition of each of the three scavengers, which suggested that $^{\bullet}OH$, h+, and $^{\bullet}O^{2-}$ were all involved in the photodegradation process.

The photocatalytic mechanism of CuPp–TiO_2 is explicated in the following description based on the above results. The valence band (VB) and conduction band (CB) energies for CuPp

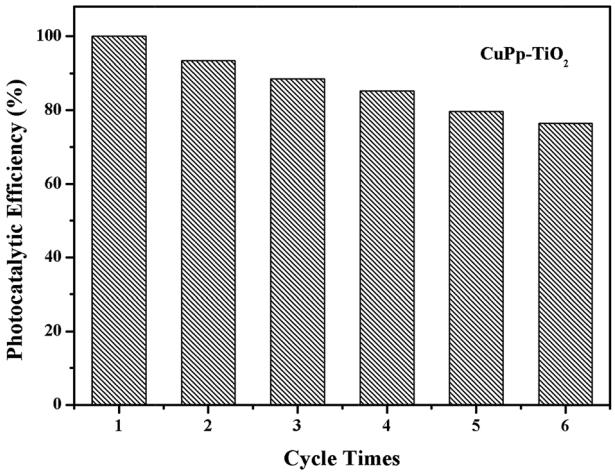

Fig. 11 Photocatalytic efficiency of the mesoporous CuPp–TiO_2 for 4-NP degradation in six cycles.

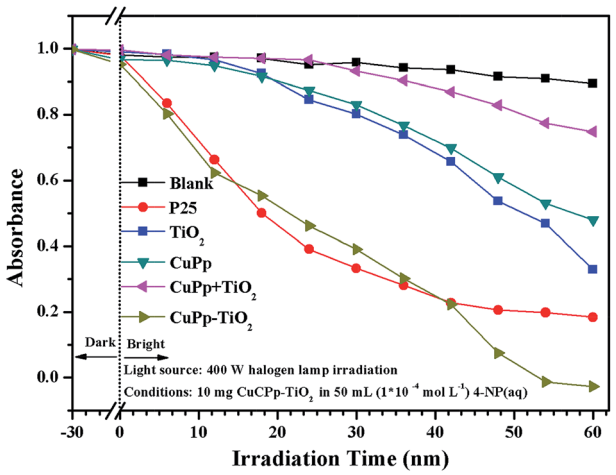

Fig. 10 Photodegradation of 4-NP *vs.* irradiation time with samples.

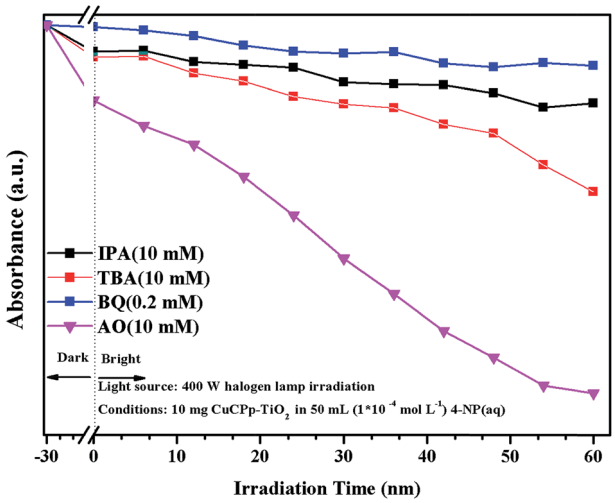

Fig. 12 Effects of some selected scavengers on the photocatalytic degradation of 4-NP over CuPp–TiO_2 composite photocatalyst under visible light irradiation.

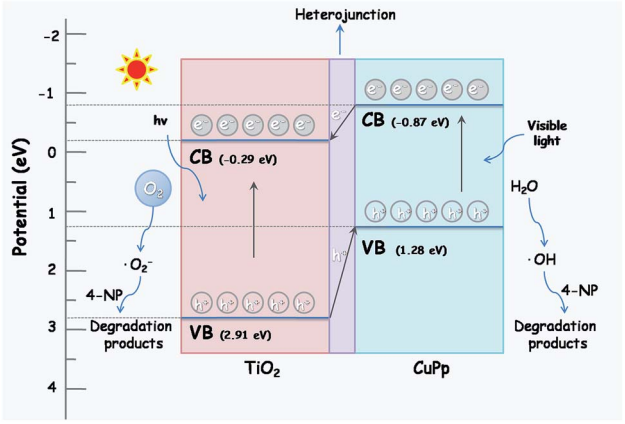

Fig. 13 The possible photocatalytic mechanism of CuPp–TiO_2 composite photocatalyst under halogen lamp irradiation.

are 1.28 and −0.87 eV respectively,[56] which is lower than that of TiO_2 (2.91, −0.29 eV). Therefore, the energy level of the excited CuPp and the CB position of TiO_2 overlap well. The electrons in VB of TiO_2 can be excited and injected into the CB of TiO_2 when the light irradiates on the surface of the photocatalyst CuPp–TiO_2. Photocatalytic activity is greatly enhanced due to the heterojunction structure in the CuPp–TiO_2 composite photocatalyst.[51,57] As shown in Fig. 13, the photogenerated electrons generated by the absorption of visible light in the CB of the CuPp migrate to the CB of the TiO_2 through the heterojunction structure forming reduction sites. The excited electrons were captured by O_2 to produce peroxyl radicals ($^{\bullet}O^{2-}$), which were capable of oxidizing 4-NP molecules. Furthermore, the photo-induced holes in the VB of TiO_2 flow to the VB of CuPp forming oxidation sites, thus resulting in the reaction with H_2O to produce $^{\bullet}OH$ and the degradation of 4-NP in the final step. Consequently, photogenerated electrons and holes are spatially isolated with high efficiency, which greatly inhibits their undesirable recombination.[38,58,59] Moreover, the mesoporous structure of CuPp–TiO_2 with large BET surface area is beneficial to pollutant adsorption and leads to more active interaction with TiO_2 and 4-NP.

4. Conclusion

A feasible route for the generation of Cu(II) porphyrin based TiO_2 composite photocatalyst with a heterogeneous structure has been comprehensively expounded in this study. Spectral techniques and gas sorption experiments have been used to characterize its spectroscopic properties and porous structures. The TiO_2 and CuPp–TiO_2 obtained by sol–gel process and solvothermal method exhibit anatase phase, as confirmed by XRD, contributing to a high efficiency of the photodegradation of 4-NP in the photocatalytic tests. CuPp–TiO_2 composite photocatalyst retained remarkable stability in photocatalysis experiments even after six cycles. It is hoped that this methodology for the porphyrin–TiO_2 photocatalyst preparation could serve as a foundation for future applications in photocatalytic degradation.

Conflicts of interest

There are no conflicts declare.

Acknowledgements

The authors acknowledge the research grant provided by the National Natural Science Foundation of China (No. 21671158) and Top-rated Discipline construction scheme of Shaanxi higher education.

References

1 A. Fujishima, *J. Photochem. Photobiol., C*, 2012, **13**(3), 169–189.
2 R. Vasilić, S. Stojadinović, N. Radić, *et al.*, *Mater. Chem. Phys.*, 2015, **151**, 337–344.
3 S. G. Kumar and L. G. Devi, *J. Phys. Chem. A*, 2011, **115**(46), 13211–13241.
4 Y. And and R. Joseph, *J. Phys. Chem. B*, 2003, **107**(43), 11970–11978.
5 A. L. Linsebigler, G. Lu and J. T. Yates, *Chem. Rev.*, 1995, **95**(3), 735–758.
6 T. H. Tran, A. Y. Nosaka and Y. Nosaka, *J. Phys. Chem. B*, 2006, **110**(50), 25525–25531.
7 Y. Kakuma, A. Y. Nosaka and Y. Nosaka, *Phys. Chem. Chem. Phys.*, 2015, **17**(28), 18691–18698.
8 S. S. Lee, H. Bai, Z. Liu and D. D. Sun, *Environ. Sci. Technol.*, 2015, **49**, 2541–2548.
9 S. Xu, H. Lu, L. Chen and X. Wang, *RSC Adv.*, 2014, **4**(85), 45266–45274.
10 D. Yu, J. Bai, H. Liang, T. Ma and C. Li, *Dyes Pigm.*, 2016, **133**, 51–59.
11 M. M. Yu, J. Li, W. J. Sun, *et al.*, *J. Mater. Sci.*, 2014, **49**(16), 5519–5528.
12 S. Bingham and W. A. Daoud, *J. Mater. Chem.*, 2011, **21**, 2041–2050.
13 J. Yu, X. Zhao and Q. Zhao, *Thin Solid Films*, 2000, **379**(1–2), 7–14.
14 Z. Xiong, L. Zhang and X. S. Zhao, *Chem.–Eur. J.*, 2014, **20**(45), 14715–14720.
15 S. Motoyama, R. Makiura, O. Sakata, *et al.*, *J. Am. Chem. Soc.*, 2011, **133**(15), 5640–5643.
16 S. Kumar, M. Y. Wani, C. Audia, C. T. Arranja, *et al.*, *J. Mater. Chem. A*, 2015, **3**(39), 19615–19637.
17 Z. Zhang, W. Y. Gao, L. Wojtas, *et al.*, *Angew. Chem.*, 2012, **51**(37), 9330–9334.
18 S. Afzal, W. A. Daoud and S. J. Langford, *ACS Appl. Mater. Interfaces*, 2013, **5**(11), 4753–4759.
19 J. Roales, J. M. Pedrosa, M. Cano, *et al.*, *RSC Adv.*, 2013, **4**(4), 1974–1981.
20 C. Wang, J. Li, G. Mele, *et al.*, *Dyes Pigm.*, 2010, **84**(2), 183–189.
21 G. Mele, E. Garcìalòpez, L. Palmisano, *et al.*, *Appl. Catal., B*, 2007, **38**(4), 309–319.
22 Y. Luo, J. Li, G. P. Yao, *et al.*, *Catal. Sci. Technol.*, 2012, **2**, 841–846.

23 L. Tasseroul, S. Lambert, M. C. Páez, *et al.*, *Dev. Brain Res.*, 2011, **44**(2), 314–318.
24 C. Wang, J. Li, G. Mele, *et al.*, Efficient degradation of 4-nitrophenol by using functionalized porphyrin-TiO_2, photocatalysts under visible irradiation, *Appl. Catal., B*, 2007, **76**(3–4), 218–226.
25 G. Mele, S. R. Del, G. Vasapollo, *et al.*, *J. Phys. Chem. B*, 2005, **109**(25), 12347–12352.
26 S. Sun, M. Pan, X. Hu, *et al.*, *Catal. Lett.*, 2016, **146**(6), 1087–1098.
27 G. P. Yao, J. Li, Y. Luo, *et al.*, *J. Mol. Catal. A: Chem.*, 2012, **361–362**(9), 29–35.
28 H. G. Yang, C. H. Sun, S. Z. Qiao, *et al.*, *Nature*, 2008, **453**, 638–641.
29 R. Wang, K. Hashimoto, A. Fujishima, *et al.*, *Adv. Mater.*, 2010, **10**(2), 135–138.
30 M. H. Yang, P. C. Chen, M. C. Tsai, *et al.*, *CrystEngComm*, 2013, **15**(15), 2966–2971.
31 L. Wang, L. Zang, J. Zhao, *et al.*, *Chem. Commun.*, 2012, **48**(96), 11736–11738.
32 M. M. Yu, C. Wang, J. Li, *et al.*, *Appl. Surf. Sci.*, 2015, **342**, 47–54.
33 X. Zhao, X. Liu, M. M. Yu, *et al.*, *Dyes Pigm.*, 2017, **136**, 648–656.
34 C. Liu, D. Yang, J. Yang, *et al.*, *ACS Appl. Mater. Interfaces*, 2013, **5**(9), 3824–3832.
35 H. Wang, X. Gao, G. Duan, *et al.*, *J. Environ. Chem. Eng.*, 2015, **3**(2), 603–608.
36 T. A. Kandiel, L. Robben, A. Alkaim, *et al.*, *Photochem. Photobiol. Sci.*, 2013, **12**(4), 602–609.
37 J. Zhang, P. Zhou, J. Liu, *et al.*, *Phys. Chem. Chem. Phys.*, 2014, **16**(38), 20377–20381.
38 A. D'Urso, M. E. Fragala and R. Purrello, *Chem. Commun.*, 2012, **43**(49), 8165.
39 H. Lin, C. P. Huang, W. Li, *et al.*, *Appl. Catal., B*, 2006, **68**(1–2), 1–11.
40 B. K. Das, S. J. Bora, M. Chakrabortty, L. Kalita, R. Chakrabarty and R. Barman, *J. Chem. Sci.*, 2006, **118**, 487–494.
41 D. Chen, D. Yang, J. Geng, J. Zhu and Z. Jiang, *Appl. Surf. Sci.*, 2008, **255**(5), 2879–2884.
42 P. Zhou, J. Yu and M. Jaroniec, *Adv. Mater.*, 2014, **26**(29), 4920–4935.
43 S. J. Zhang, *Ultrason. Sonochem.*, 2012, **19**(4), 767–771.
44 J. Yu, G. Dai, Q. Xiang, *et al.*, *J. Mater. Chem.*, 2011, **21**(4), 1049–1057.
45 D. A. H. Hanaor and C. C. Sorrell, *J. Mater. Sci.*, 2011, **46**(4), 855–874.
46 H. Wang, D. Zhou, S. Shen, *et al.*, *RSC Adv.*, 2014, **4**, 28978–28986.
47 A. I. Carrillo, E. Serrano, J. C. Serrano-Ruiz, *et al.*, *Appl. Catal., A*, 2012, **435–436**(17), 1–9.
48 W. Xuan, C. Zhu, Y. Liu, *et al.*, *Chem. Soc. Rev.*, 2012, **41**(5), 1677–1695.
49 L. L. He, Z. F. Tong and Z. H. Wang, *J. Colloid Interface Sci.*, 2018, **509**, 448–456.
50 H. Huang, N. Huang and Z. H. Wang, *J. Colloid Interface Sci.*, 2017, **502**, 77–88.
51 J. Shu, Z. Wang, G. Xia, Y. Zheng, *et al.*, *Chem. Eng. J.*, 2014, **252**, 374–381.
52 N. Serpone, *Sol. Energy Mater. Sol. Cells*, 1995, **38**, 369–379.
53 Y. N. Wang, K. J. Deng and L. Z. Zhang, *J. Phys. Chem. C*, 2011, **115**, 14300–14308.
54 L. Q. Ye, K. J. Deng, F. Xu, L. H. Tian, T. Y. Peng and L. Zan, *Phys. Chem. Chem. Phys.*, 2012, **14**, 82–85.
55 X. P. Song, Q. Yang, X. H. Jiang, M. Y. Yin and L. M. Zhou, *Appl. Catal., B*, 2017, **217**, 322–330.
56 W. J. Sun, J. Li, G. Mele, *et al.*, *J. Mol. Catal. A: Chem.*, 2013, **366**(1), 84–91.
57 H. Wang, L. Zhang, Z. Chen, *et al.*, *Chem. Soc. Rev.*, 2014, **43**(15), 5234–5244.
58 J. Low, J. Yu, M. Jaroniec, *et al.*, *Adv. Mater.*, 2017, **29**(20), 1601694–1601714.
59 J. Yu, J. Low, W. Xiao, P. Zhou and M. Jaroniec, *J. Am. Chem. Soc.*, 2014, **136**, 8839–8842.